Environ Geol (2009) 58:1575–1585
DOI 10.1007/s00254-008-1664-7

ORIGINAL ARTICLE

Geochemical investigation of groundwater in a Granitic Island: a case study from Kinmen Island, Taiwan

Tai-Sheng Liou · Hsueh-Yu Lu · Cheng-Kuo Lin · Wayne Lin · Yu-Te Chang · Jeng-Ming Chien · Wen-Fu Chen

Received: 24 September 2008 / Accepted: 18 November 2008 / Published online: 6 January 2009

Abstract Kinmen Island is principally composed of low permeable granitoid and covered by a very thin sedimentary layer. Both surface and groundwater resources are limited and water demand is increasing with time. The groundwater in the granitoid has been surveyed as an alternative water source for daily use. Two to five highly fractured zones in the granitoid aquifer for each site were first determined by geochemical well logging. Accordingly, ten samples were collected from three sites. Using environmental isotopes and geochemical modeling, geochemical processes occurring due to water–rock interaction in the granitoid aquifer can be quantitatively interpreted. The stable isotopes of oxygen and hydrogen in groundwaters cluster along Taiwan's local meteoric waterline, indicating evaporation does not have considerable effect on groundwaters. Given such a high evaporation rate for Kinmen Island, this result implies that infiltration rate of groundwater is high enough to reduce retention time through a well-developed fracture zone. NetpathXL is employed for inverse geochemical modeling. Results determine gypsum as being the major source of sulfate for deep groundwaters. The contribution from pyrite is minor. In addition, the weathering of albite to kaolinite is the dominant water–rock interaction characterizing geochemical compositions of deep groundwater in Kinmen Island.

Keywords Granitoid aquifer · Environmental isotopes · Geochemical modeling · Factor analysis · Kinmen Island

T.-S. Liou · H.-Y. Lu (✉)
Department of Earth and Environmental Sciences,
National Chung Cheng University,
168, University Rd., Min-Hsiung, Chia-Yi, Taiwan
e-mail: seishei@eq.ccu.edu.tw

C.-K. Lin · W. Lin · Y.-T. Chang · J.-M. Chien
Resource Technology Division, Energy and Environmental Research Laboratories, Industrial Technology Research Institute,
Hsin-Chu, Taiwan

W.-F. Chen
Department of Tourism Management,
Chia Nan University of Pharmacy and Science,
Tai-nan, Taiwan

Introduction

Kinmen is an island located approximately 10 km east of Xiaman City, China and 200 km off the western coast of Taiwan (Fig. 1). It has a population of about 50,000 and the land area is 150 km^2. Generally, the climate of Kinmen Island is semi-arid. Annual precipitation and evaporation are 1,072 and 1,661 mm, respectively. Evaporation normally exceeds rainfall in 9 months of the year; therefore, the seven creeks on the island are all ephemeral and the reservoirs are not able to provide a stable water supply for daily usage of residents and agricultural irrigation. Consequently, the island has shown an increase in the amount of groundwater annually pumped for decades. The proportion of groundwater used in general water supply is about 50%; 16 small reservoir lakes provide the rest. Overpumping of groundwater has caused significant drop in groundwater level and subsequent seawater intrusion is increasingly degrading groundwater quality. In more recent years, the county government has supported sustainable tourism business development; however, tourism numbers are compounding the problem. Therefore, the long-term protection of groundwater resources is of high-priority concern. Since 2000, the government has undertaken fundamental investigations of the hydrogeological system. The granitoid aquifer is being considered first as a potential

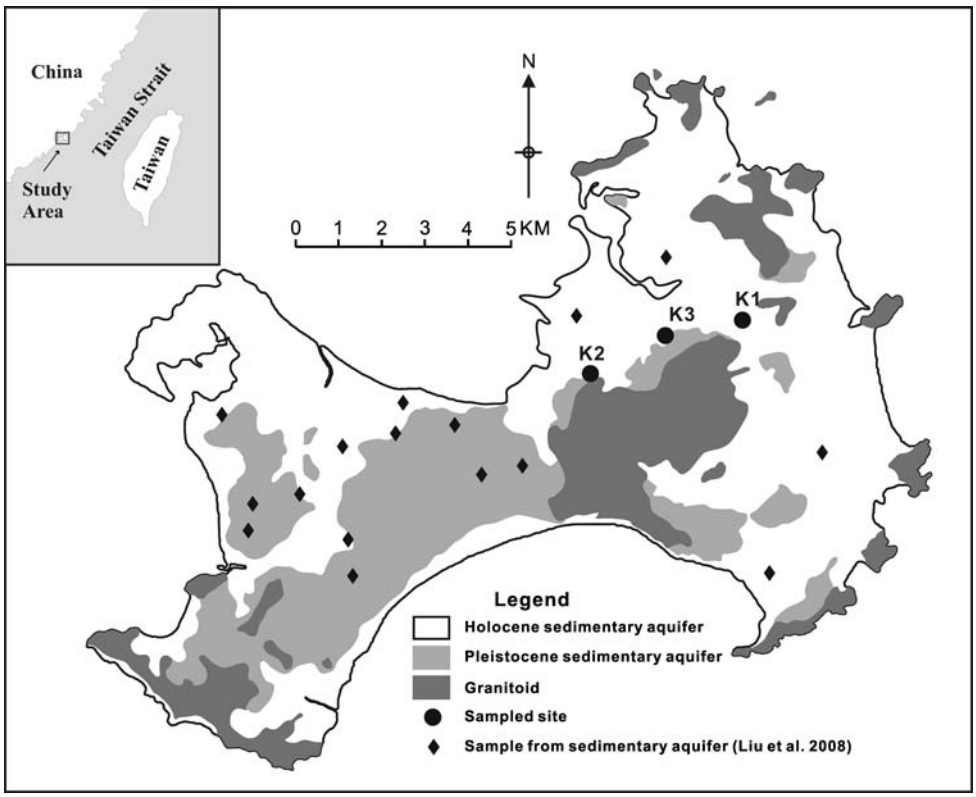

Fig. 1 Geological map of Kinmen Island showing the three sampled sites (K1–K3)

water resource; however, it is very costly to perform hydrogeological surveys in fractured rock aquifers. Fortunately, Taiwan Power Company has provided full financial support to construct deep monitoring wells and all related geophysical and geochemical investigations.

Study area

Hydrogeological background

The geology of Kinmen Island is characterized by extensive Yanshanian magmatism, which is commonly regarded as an active continental margin related to subduction of the Kula or Izanagi plate under Eurasia in the periods of Jurassic and Cretaceous. These granitoids of Yanshanian magmatism formed the basement of the island. Since 100 Ma, the area has been subjected to a geodynamic extension. The upwelling of lithospheric mantle promoted mafic magmatism instead of granitic magmatism during Yanshanian. At this stage, high-angle extensional fractures and faults developed; and gabbro dikes intruded the Mesozoic granitoid basement along these pathways. The western part of Kinmen Island subsequently became a graben receiving sediments mainly from SE China. The topographic elevation remained relatively high in the eastern part of the island. Therefore, the thickness of overlying Tertiary and Quaternary sedimentary fills ranges from more than 150 m in the west to less than a few meters in the east. The simplified stratigraphic sequence is tabulated in Table 1 (Lin et al. 1997).

Table 1 Stratigraphic column of Kinmen Island (Lin et al. 1997)

Age		Lithology
Quaternary	Holocene	Conglomerate with mud and sand beds
	Pleistocene	Lateritized conglomerate
Tertiary	Pliocene	
	Miocene	Lateritized basalt and underlying fresh basalt
	Oligocene	Sandstone with mud and conglomerate beds
	Eocene	
Cretaceous	Cretaceous	Granite and granitic gneiss with abundant gabbro dikes
Jurassic	Jurassic	Quartz schist and quartzite

Because the granitoid basement has low hydraulic conductivity, sedimentary aquifers are the major reservoirs of groundwater. As shown in Fig. 2, the sedimentary aquifer gradually thins out from west to east. Generally, sedimentary aquifers can be divided into three areas by the largest outcrop of granitoid basement named as Taiwu Mountain, which is the highest summit located in the mid-eastern island. The groundwater in the western island (area A) flows radially from the central area to the coastline. The other two smaller areas (B in the southeast and C in the

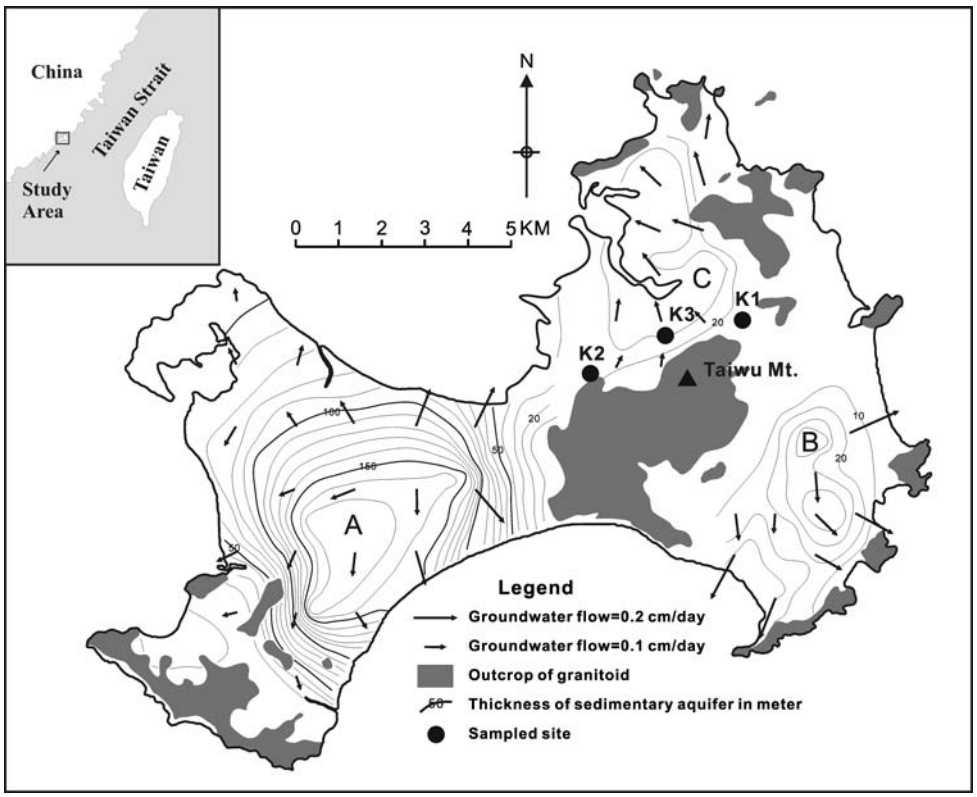

Fig. 2 Contour map of sedimentary aquifer in Kinmen Island (Liu et al. 2006)

northeast) in the eastern part of the island are generally recharged around Taiwu Mountain and discharged along the coastline (Liu et al. 2006). However, sedimentary aquifers in areas B and C are much thinner than those in area A. According to the results of pumping and slug tests from Rechang Consulting Company (2002), the hydraulic conductivities of sedimentary aquifers are in the range of 10^{-2} to 10^{-3} cm/s in areas A and B, and 10^{-3} to 10^{-4} cm/s in area C.

According to an investigation and numerical simulation of Liu et al. (2006), from May 2002 to April 2003, the annual infiltration rate is 15.40 Mm^3 ($\times 10^6$ m^3), which is 7% of total precipitation, while total loss of groundwater is 17.91 Mm^3 including 15.13 Mm^3 withdrawn from production wells and 2.78 Mm^3 outflowing to the coastline. Therefore, the aquifers demonstrate a negative balance on storage and observed average groundwater level has decreased about 0.237 m during this period. Based on this information, an alternative water resource is a very important issue to Kinmen Island.

Groundwater quality of sedimentary aquifers

Liu et al. (2008) have performed a detailed survey for characterizing groundwater quality using multivariate analysis and geochemical modeling. The groundwaters collected from May 2002 to April 2003 show typical characteristics of freshwater with low TDS ranging from 66 to 602 mg/l (Fig. 1). Information regarding alkalinity is not available; hence, the geochemical type of water cannot be identified. However, Liu et al. (2008) found a salinization factor, which explains 42.33% of the total variance in factor analysis. There are strong positive loadings on electric conductivity (EC), TDS, SO_4, Cl, Ca, Mg, Na and K, which are all major components in seawater; and Na is highly correlated with Cl ($r^2 = 0.82$). It is considered the result of mixing with leachate of marine sediments because the groundwater level is not lower than seawater level and the spatial distribution of the scores of the salinization factor does not demonstrate considerable correlation to seawater intrusion. Factor 2 is an indicator of a redox environment. It explains 23.74% of the total variance with strong absolute loadings of Eh, pH, NO_3, dissolved oxygen (DO), Fe, and Mn. The groundwaters of sedimentary aquifers in Kinmen Island are under highly oxidizing conditions with Eh values ranging from 393 to 507 mV, implying retention times may be short.

Groundwaters in sedimentary aquifers have lower pH values (4–5) than precipitations (5.5). Liu et al. (2008) proposed a geochemical water–rock interaction system in weathered granitoids with mineral assemblage of aluminum oxide (Al_2O_3), kaolinite ($Al_2Si_2O_5(OH)_4$), quartz (SiO_2) and magnetite (Fe_3O_4) to interpret the situation whereby pH value decreases while Eh value increases in

sedimentary aquifers (Chen et al. 2004; Lin et al. 1997; Parkhurst and Appelo 1999).

Methods

Groundwater sampling and geochemical analysis

Groundwater collected from an unlined borehole, which filters the whole aquifer, generally gives an average groundwater concentration and does not permit good comprehension of possible vertical distributions of geochemical properties. On the other hand, the multi-level sampling method with a double-packer system allows for withdrawing groundwaters which are representative of chemical compositions from multiple target depths. The double-packer equipment used in this study consists of two rubber sheaths linked by aluminum perforated pipe, in which the pumping module and geophysical well logger are installed. The pumping module is operated by a programmable logic controller (Mitsubishi AL-10MR-D PLC system) and a 2-HP air compressor (TIGER). The equipment can collect water samples from down to 700-m depth. Water that remains in the well between sampling periods is unrepresentative of water in the aquifer formation. Prior to collecting samples, the wells were purged for at least 10 days, which was equivalent to over 40 well volumes of stagnant water. A drainage system was constructed to prevent purged stagnant water from flowing back into well. During well purging, water qualities were monitored by Hydrolab Minisode 4a.

Geochemical logging was performed both before and after purging wells with an Idronaut Ocean Seven 320 multiparameter CTD (Conductivity, Temperature, Depth) probe, which measures: temperature, pH, DO, EC, and redox state. Downhole log data were recorded at 5-m depth intervals.

Comparing geochemical logs before and after well purging, allows for highly fractured zones to be identified. Then, the double-packer system was applied to seal a 2-m-thick interval at the target depth. Representative formation water samples in the isolated portions were subsequently collected after purging at least three volumes of stagnant water and the fundamental geochemical properties of: temperature, pH, DO, EC, and the redox state were simultaneously measured by Idronaut Ocean Seven 320. The extracted groundwater was filtered through 0.45 μm glass fiber paper and collected by HDPE bottles to avoid boron contamination from borosilicate-glass containers. Filtered water samples underwent anion analysis measured by HACH spectrophotometer. For cation analysis, samples were preliminarily acidified with ultrapure nitric acid to pH 4 and measured by Induced Coupled Plasma-Atomic Emission Spectroscopy (ICP-AES).

Some water samples were also collected for determination of stable isotopic compositions of oxygen and hydrogen. Oxygen-18 ($\delta^{18}O$) was determined using CO_2 gas that has equilibrated with water at a constant temperature (Epstein and Mayeda 1953). The equilibrated CO_2 gas was measured by a VG SIRA 10 isotope ratio mass spectrometer. Hydrogen gas was produced by reduction of water with zinc metal. The δD value of the hydrogen was then measured using a dual-inlet isotope ratio mass spectrometry (VG MM602D) (Coleman et al. 1982). Both analyses were conducted at the Isotope Hydrology Laboratory of Academic Sinica, Taipei, Taiwan.

Geochemical modeling

Geochemical modeling is a powerful technique for characterizing geochemical phenomena and predicting their evolution in time as well as in space when coupled with flow modeling. Many programs have been developed to perform a wide variety of aqueous geochemical calculations. NETPATH, designed by the USGS, is one of the most popular softwares for aqueous geochemical modeling (Plummer et al. 1994). A revised version, NetpathXL, is designed to work with EXCEL spreadsheet (Parkhurst and Charlton 2008). The code is based on an ion-association aqueous model and has capabilities for speciation, saturation-index calculations, isotope fractionation, and inverse modeling. In this study, NetpathXL is employed to calculate the chemical mass transfer that has occurred during the interaction between groundwater and granitoid.

Results and discussion

Identification of highly fractured zone

Three deep wells were constructed in the eastern part of Kinmen Island, which is relatively high in elevation and covered by thin sedimentary aquifers (Fig. 2). Prior to sample collection, the highly fractured zone in the granitoid rock must be identified. Traditionally, geophysical methods are used to image contrast rock properties relating to fracturing. However, fracturing alone does not necessarily indicate an increase in permeability. In this study, the geochemical well logs measured before and after well purging were utilized to identify the permeable layers. The dewatering of formation water due to pumping may enhance the geochemical contrast, which indicates the position of a highly permeable zone. Accordingly, a few highly permeable zones are identified as shown in Fig. 3. The subsequent double-packer pumping test demonstrates that the hydraulic conductivities in these fractured zones are in the range of 2.2×10^{-4} to 1.2×10^{-3} cm/s,

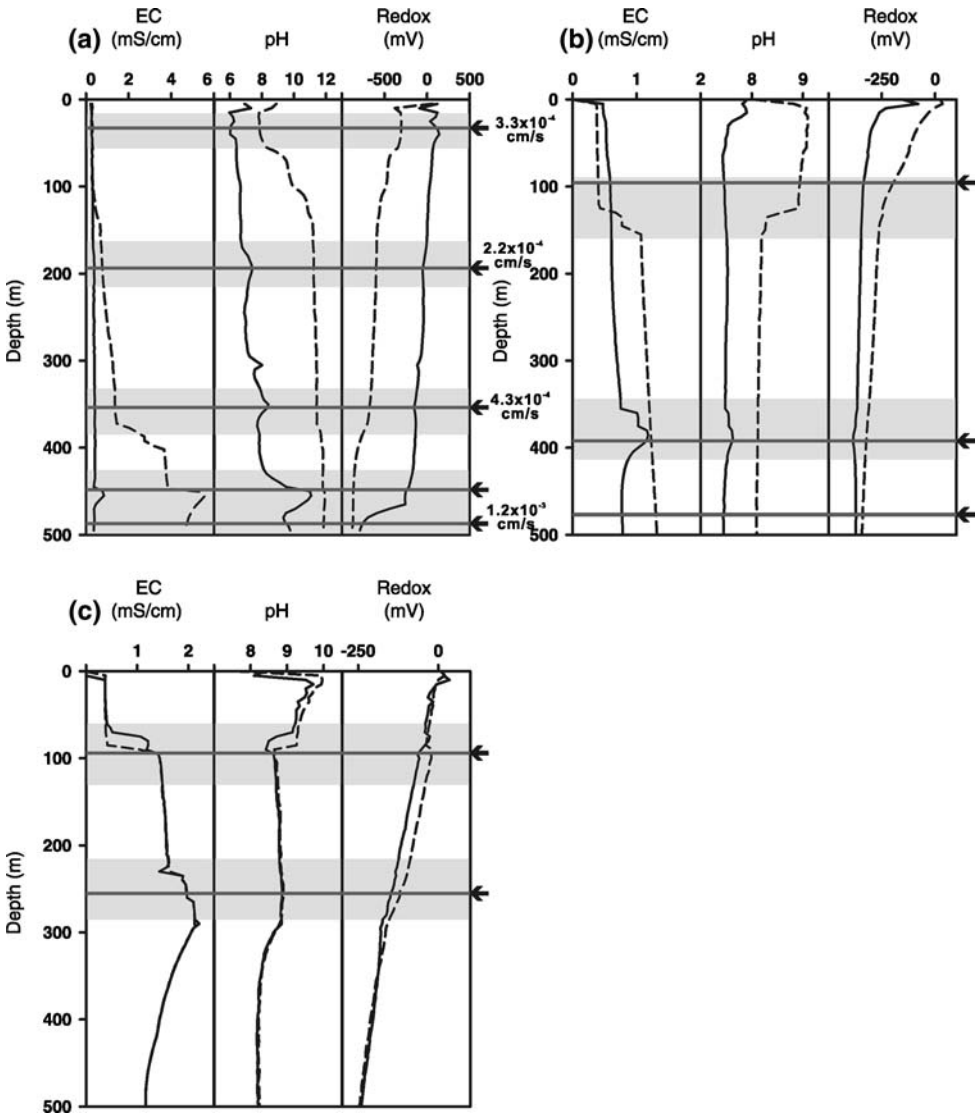

Fig. 3 Well logs of three sites: **a** K1, **b** K2 and **c** K3. The *dashed line* and *solid line* denote the well logs before and after well purge, respectively. The *shadow zone* represents the range with considerable change of well logs before and after well purge. The *arrow symbol* indicates the sampling depth and hydraulic conductivity is shown next to arrow

which can be considered as permeable layer (Fig. 3). In addition, geophysical well logs and downhole video images (not shown here) also help to distinguish highly fractured zones, which are potentially enriched with water resources (Fig. 3). Ten groundwater samples were collected for geochemical analysis from these identified intervals at three sites. The samples are coded by a "K" (for Kinmen) followed by one-digit site number and one-digit screening number; for example, K1-1. The lower the screening number, the shallower the sample is.

Geochemical interpretations

The results of geochemical analysis of ten groundwater samples from three sites are listed in Table 2. Samples both from sedimentary aquifers (Liu et al. 2008) and granitoid aquifers (this study) are included in the subsequent multivariate statistical analysis. Factor analysis extracts four factors (eigenvalue > 1) to account for 88.33% of the total variance as shown in Table 3 and the rotated loadings of varimax normalized factor matrix for the four-factor model are given in Table 4. As with the aforementioned results from sedimentary aquifers (Liu et al. 2008), there are two major factors representing seawater salinization and redox states. In the results from all groundwaters, factor 1 and factor 2 can be combined into seawater salinization factor and factor 3 and factor 4 are equivalent to the redox factor. These differences demonstrate that the geochemical interaction between groundwater and granitoid has considerable effect on water quality if the sedimentary aquifer and granitoid aquifer were recharged by local precipitations having similar chemical compositions. This requires further discussion.

Table 4 shows that factor 1 has high positive loadings on EC, SO_4, Ca, and Na, but very low loadings on Cl and K. On the contrary, the values of EC of groundwaters in

Table 2 Geochemical and isotopic compositions of groundwaters in granitoid aquifer[a]

Sample	K1-1	K1-2	K1-3	K1-4	K1-5	K2-1	K2-2	K2-3	K3-1	K3-2
Depth (m)	37.1–40.1	195.1–198.1	351.1–354.1	440.1–443.1	489.1–492.1	94.1–96.3	389.9–392.1	478.7–480.9	94.0–96.0	258.5–260.5
T (°C)	23.2	26.0	28.9	31.4	31.4	24.0	29.4	31.1	24.5	27.7
EC(mS/cm)	0.271	0.292	0.376	0.333	0.321	0.401	1.358	2.124	1.119	2.031
pH	6.71	6.29	6.92	9.44	9.76	7.64	8.09	8.19	8.35	8.83
Redox (mV)	−44	151	−206	−668	−666	−334	−538	−541	−209	−630
HCO_3	53.2	37.5	67.6	54.0	46.6	142.7	46.7	28.9	25.0	5.2
PO_4	2.17	0.31	0.17	0.185	0.3	0.38	0.205	0.23	0.36	0.17
SO4	9	13	11	4	13	1	530	830	550	790
NO_3	1.40	1.70	0.40	0.35	0.30	0.40	1.45	0.60	Nd	0.15
NO_2	0.079	0.002	0.002	0.001	0.002	0.027	0.013	0.022	0.018	0.012
NH_3	0.145	1.870	0.045	0.465	0.890	0.190	0.395	0.220	0.590	0.035
SiO_2	6.0	5.0	5.7	4.6	5.8	40.4	15.6	14.2	20.6	17.3
F	0.52	0.92	0.83	2.62	1.95	1.69	3.17	3.27	4.78	7.18
Cl	40.2	45.2	43.4	22.6	30.8	41.0	92.8	115.4	51.4	43.6
Fe	0.13	0.58	0.77	0.16	0.63	0.48	0.53	0.51	0.04	0.04
Mn	0.31	0.33	0.37	0.012	0.17	0.29	0.05	0.13	0.02	0.01
Ca	16.1	19.6	26.8	5.93	14.5	41.0	103.0	159.0	123.0	210.0
Mg	3.17	4.10	3.73	0.27	0.53	3.43	1.20	1.52	1.94	Nd
Na	11.6	16.2	17.2	27.4	26.8	32.2	109.0	154.0	126.0	102.0
K	3.28	4.66	4.48	2.33	4.43	2.68	2.72	3.38	4.19	2.45
Cu	0.004	0.007	0.008	0.004	0.046	0.004	ND	0.002	0.003	ND
Cd	ND	ND	ND	0.001	0.006	ND	ND	ND	ND	ND
Cr	0.003	0.002	0.001	ND	0.013	ND	ND	ND	ND	ND
Ni	2.62	2.40	3.28	1.75	2.13	0.03	ND	ND	ND	ND
Pb	0.018	0.008	ND	0.016	ND	ND	ND	ND	ND	ND
Zn	0.04	0.46	0.93	0.15	0.10	0.05	0.02	0.07	0.02	0.01
As	ND	ND	ND	ND	0.0007	Nd	Nd	0.0004	0.0012	ND
$\delta^{18}O$	−25.7	−38.1	−41.5	−43.0	–	–	–	–	–	–
δD	−6.37	−8.12	−8.53	−8.76	–	–	–	–	–	–

ND not detected, not determined

[a] All geochemical concentrations are in mg/l

Table 3 Extracted factors (eigenvalue > 1) in the factor analysis; and their eigenvalue, percentage of variance and cumulative percentage of variance

Factor	Eigenvalue	Percentage of Total variance	Cumulative eigenvalue	Cumulative percentage of variance
1	4.86	40.49	4.86	40.49
2	3.02	25.18	7.88	65.67
3	1.62	13.52	9.50	79.19
4	1.10	9.14	10.60	88.33

sedimentary aquifers present good linear relationship both with SO_4 and Cl (Liu et al. 2008). However, Cl and K are relatively enriched and conserved components in seawater. It is less possible to consider a factor (factor 1) without a high loading of Cl and K as seawater mixing. In addition, the highest loadings in factor 1 are 0.94 for EC and SO_4. This can be explained by EC values of groundwaters being controlled by SO_4 content. Therefore, factor 1 for groundwaters from the granitoid aquifer should be designated as being SO_4 sourced but not seawater mixing. Under this situation, factor 2 should be interpreted as halite (NaCl) dissolution. Although Na and Cl do not belong to the same factor (Table 4), this can be explained by presenting an additional Na source other than halite. The Na source will be discussed in the following inverse geochemical modeling.

As mentioned earlier, the redox state factor for groundwaters from the sedimentary aquifer is split into factor 3 and factor 4 in this study (Table 4). Liu et al. (2008) concluded that redox state factor is caused by nitrogenous fertilizers for agricultural uses, and, the subsequent water–rock interaction in granitoid involve mass transfer of the components in factor 3 to complicate the redox state factor.

Table 4 Varimax rotated factor loading matrix

Variables	Factor 1	Factor 2	Factor 3	Factor 4
EC	**0.94**	0.19	0.13	0.20
pH	0.29	0.01	0.07	**0.91**
Eh	−0.36	0.17	−0.12	**−0.86**
SO_4	**0.94**	−0.10	0.11	0.26
NO_3	−0.07	−0.04	0.38	**−0.74**
Cl	0.38	**0.81**	−0.01	−0.29
Fe	−0.10	−0.09	**−0.91**	−0.07
Ca	**0.91**	0.03	0.14	0.29
Mg	−0.06	**0.73**	0.16	−0.57
Na	**0.88**	0.33	0.16	0.03
K	0.06	**0.89**	0.06	0.30
Mn	−0.25	−0.03	**−0.82**	0.16

Significant loadings are underline

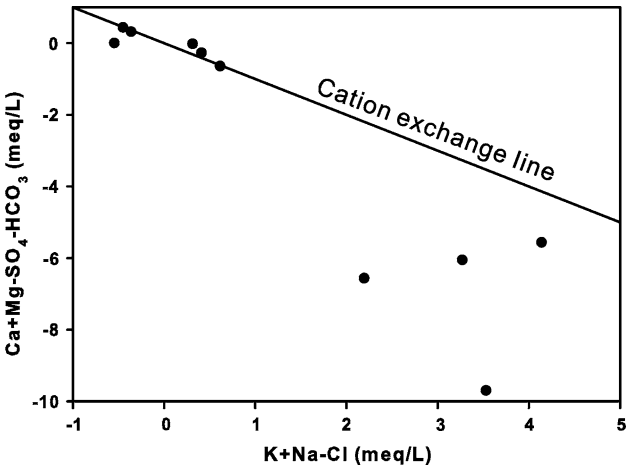

Fig. 4 Relation between Ca + Mg–SO_4–HCO_3 and Na + K–Cl in the groundwaters from the granitoid aquifer. The straight line with a slope of −1 shows cation exchange between Ca + Mg and Na + K

To evaluate the effect of cation exchange, the bivariate plot of Ca + Mg–SO_4–HCO_3 as a function of Na + K–Cl is used (Jalali 2005, 2007). The value of Ca + Mg–SO_4–HCO_3 represents the amount of Ca and Mg gained or lost from gypsum, calcite and dolomite, while that of Na + K–Cl is related to the amount of Na and K gained or lost from halite. If dissolution and precipitation of these minerals are the only significant processes determining chemical composition, the data should be clustered around the original point. Furthermore, a linear relation with a slope of −1 will develop when cation exchange between Ca/Mg and Na/K has considerable effect on chemical composition. Figure 4 demonstrates that samples with low SO_4 content are plotted around the cation exchange line, and the samples with high SO_4 content are located below the line, which means that there is an additional source providing excess SO_4.

The oxidation of pyrite (FeS_2) and dissolution of gypsum ($CaSO_4 \cdot 2H_2O$) are generally considered the major source of SO_4 in groundwater if no mixing of seawater and geothermal water is involved (Stober and Bucher 1999; Beaucaire et al. 1999). It has been also proposed that Cl and SO_4 may originate from fluid inclusions in quartz that are released by fracture formation, weathering or other processes (Peters 1986; Gascoyne 1994). However, Cl and SO_4 do not have high loading on the same factor (Table 4) and there is no report to demonstrate a SO_4 source from fluid inclusion in Kinmen granitoids (Chen 1984; Lan et al. 1997). Therefore, pyrite in granitoid and/or gypsum precipitated in topsoil is the most likely sources of SO_4.

Isotope geochemistry

The stable isotopes ($\delta^{18}O$ and δD) of four groundwater samples from K1 were also analyzed and the results are

listed in Table 2. This information provides more detailed interpretation on geochemical evolution. Generally, the variation of stable isotopes with depth is not distinct except in shallow groundwater (K1-1), which contains heavier isotopic compositions. It can be considered as the result of seasonal variation; and the mixing process gradually reduces seasonal variation of isotopic composition with depth (Clark and Fritz 1997). The values of stable isotopes also demonstrate that there is no considerable effect on geochemical property from seawater ($\delta^{18}O = 0‰$ and $\delta D = 0‰$). The derivation is *similar* to that from general geochemical interpretations.

Figure 5 demonstrates that the values of stable isotopes located on Taiwan's local meteoritic water line (LMWL) (Liu 1984). Evaporation did not make considerable fractionation between $\delta^{18}O$ and δD during infiltration; otherwise, the isotopic compositions would evolve off the LMWL to another line with gentle slope (Craig et al. 1963). Obviously, groundwater should suffer evaporation during infiltration, as the mean annual evaporation is 1,235 mm, which is much higher than the mean annual precipitation (977 mm in the same period). Under these constraints, the groundwaters from granitoid aquifers should be involved with the evaporation process under high humidity whilst the infiltration rate should be high enough to reduce retention time in vadose zone. This can be characterized by fast infiltration through well-developed fractures in hard-rock provinces like the granitoid in the study area.

Inverse geochemical modeling

According to the derivation from geochemical interpretations, inverse geochemical modeling can be utilized to quantitatively simulate hydrochemical evolution of groundwater. Mineral stability diagrams are first used to help define reactions controlling water chemistry (Tardy 1971). Figure 6 demonstrates mineral stability fields for a weathering albite system (Na_2O–Al_2O_3–H_2O–SiO_2) (Fig. 6a) and K-feldspar system (K_2O–Al_2O_3–H_2O–SiO_2) (Fig. 6b), which are two major mineralogical components in granitoids. Three groups of groundwater can be categorized in the figure. For Group 1, shallow groundwaters from K1 (K1-1, K1-2 and K1-3), albite and K-feldspar are all weathered into kaolinite. The reactions can be described by:

$$\underset{\text{Albite}}{2NaAlSi_3O_8} + 2H^+ + 9H_2O \leftrightarrow 2Na^+ + 4H_4SiO_4 + \underset{\text{Kaolinite}}{Al_2Si_2O_5(OH)_4} \quad (1)$$

$$\underset{\text{K}-\text{felspar}}{2KAlSi_3O_8} + 2H^+ + 9H_2O \leftrightarrow 2K^+ + 4H_4SiO_4 + \underset{\text{Kaolinite}}{Al_2Si_2O_5(OH)_4} \quad (2)$$

For Group 2, deep groundwaters from K1 (K1-4 and K1-5), albite and K-feldspar alter to gibbsite and muscovite, respectively. The simplified geochemical reactions to describe these processes are

$$\underset{\text{Albite}}{NaAlSi_3O_8} + H^+ + 7H_2O \leftrightarrow Na^+ + 3H_4SiO_4 + \underset{\text{Gibbsite}}{Al(OH)_3} \quad (3)$$

$$\underset{\text{K}-\text{felspar}}{3KAlSi_3O_8} + 2H^+ + 12H_2O \leftrightarrow 2K^+ + 6H_4SiO_4 + \underset{\text{Muscovite/Illite}}{KAl_3Si_3O_{10}(OH)_2} \quad (4)$$

The groundwaters with high SO_4 content are all in Group 3. Kaolinite is the most stable phase for the albite system as reaction (2); and, for the K-feldspar system, the stability field locates along the boundary between kaolinite and illite (Fig. 5b). The illite-producing reaction can be also described by reaction (4). In addition, oxidation of pyrite is one of the possible sources of SO_4. Although the formation of iron hydroxide is dependent on the pH and redox state, a completed oxidation of pyrite can be described by

$$\underset{\text{Pyrite}}{2FeS_2} + 7H_2O + 7.5O_2 \rightarrow \underset{\text{Iron hydroxide}}{Fe(OH)_3} + 4SO_4^{2-} + 8H^+ \quad (5)$$

All of these phases are included in the inverse geochemical modeling but gibbsite is excluded because the information of Al content in groundwater is not available.

In this study, NetpathXL is used to model the potential sources of SO_4 in K2 and K3. Therefore, a geochemical reaction system is established concentrating on the mass balance of SO_4. Based on the geochemical interpretations and phase stability, four categories of phases are considered to be involved in rock–water interaction:

1. Evaporitic minerals include gypsum, calcite, dolomite and halite, which are highly soluble and can enter and exit groundwater system in the model.

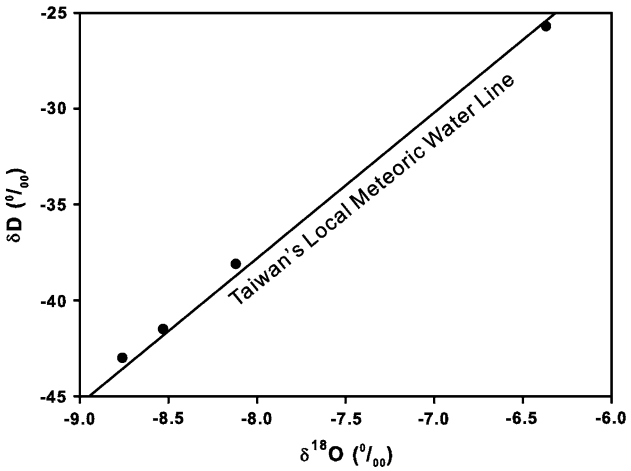

Fig. 5 Plot of δD versus $\delta^{18}O$ of groundwater. The straight line represents Taiwan's local meteoric water line (Liu 1984)

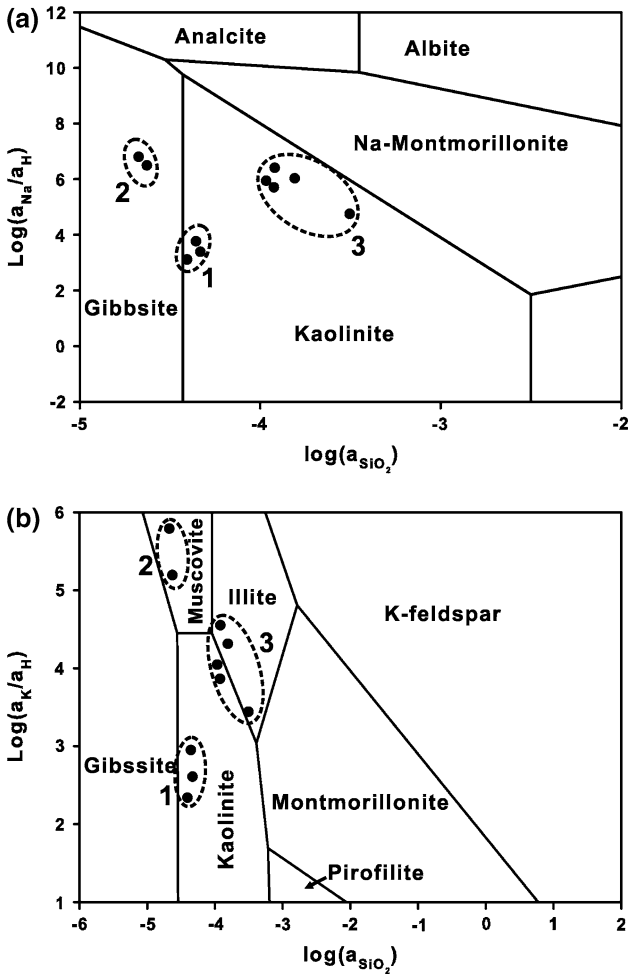

Fig. 6 Phase diagrams showing the aqueous geochemical conditions for **a** Na_2O–Al_2O_3–H_2O–SiO_2 system, and **b** K_2O-Al_2O_3–H_2O–SiO_2 system. Group 1 shows that kaolinite is the most stable phase for shallow groundwater; Group 2 demonstrates that albite and K-feldspar in granitoid are weathered into gibbsite and muscovite, respectively, and Group3 represents groundwaters from K2 and K3 containing high SO_4

2. Major mineral assemblages in granitoid include pyrite, quartz, K-feldspar, albite and biotite, which are forced to dissolve. Quartz (or aqueous silica) is a potential product in the alteration of albite and K-feldspar; therefore, both dissolution and precipitation processes are allowed for SiO_2.
3. Products of weathered granitoid include kaolinite, illite and iron hydroxide, which are precipitation only in the simulation. Muscovite, the stable phase in Group 2, is excluded from the model because the chemical composition of muscovite is similar to illite.
4. CO_2 is a very common phase in geochemical reactions of groundwater system. In addition, the redox state is a factor that must be included in the redox reactions as suggested by Plummer et al. (1994).

The elements involved in these modeled phases, including: S, Ca, Mg, Na, K, Fe, Si, C and Cl are designated as mass balance constraints.

The model simulates phase transfer by assuming that groundwater flow from K2-1 to K2-3. Sample K2-3 has the highest concentration of SO_4 and is considered as the final solution. K2-1 is the shallow groundwater at the same site and may represent the recharging source of K2-3. The simulation obtains 12 possible models as shown in Table 5.

There are some findings that can be further examined to obtain a better model for geochemical evolution of groundwater:

1. The amount of pyrite dissolution is small in all models and no model can be obtained if gypsum was removed from the phase list of the simulation. Therefore, gypsum dissolution is the dominant process for the groundwater with high SO_4 concentration (Model 1-6) and pyrite oxidation can be ignored (Model 7–12).
2. In Models 5 and 6, calcite must be removed from the groundwater if dolomite is dissolved. It is less possible because calcite and dolomite are similar in geochemical properties and they are usually associated with each other.
3. The resultant models demonstrate that kaolinite is incompatible with SiO_2, which means the major product of weathered granitoid is either kaolinite (Model 1 and 2) or SiO_2 (Model 3 and 4). However, the mineral stability diagram shows kaolinite is the stable phase for K2-1 and K2-3 (Fig. 6). It supports Models 1 and 2 as being more plausible than the others.
4. The difference between Models 1 and 2 is not considerable.

According to these discussions, the conceptual model of the geochemical reactions governing the mass transfer of water–rock interaction can be described by

$$\begin{aligned} &\mathrm{K2-1} + \mathrm{Gypsum} + \mathrm{Albite} + (\mathrm{K-feldspar}) + \mathrm{Halite} \\ &\quad + (\mathrm{Biotite}) + \mathrm{CO_2} \\ &\quad \rightarrow \mathrm{K2-3} + \mathrm{Calcite} + (\mathrm{Dolomite}) + \mathrm{Kaolinite} \\ &\quad + (\mathrm{Illite}) + (\mathrm{Iron\,hydroxid}) \end{aligned} \quad (6)$$

where the amount of the bracketed phases are relatively minor. This result also confirms that there is an additional source of Na (albite weathering) other than halite to separate Na and Cl into two factors in factor analysis.

Conclusions

According to geochemical well logging, highly fractured zones were identified in granitoid aquifers and ten groundwater samples were collected for isotope and

Table 5 The mass transfers of 12 possible models obtained from inverse geochemical simulation

Phase	Model 1	Model 2	Model 3	Model 4	Model 5	Model 6	Model 7	Model 8	Model 9	Model 10	Model 11	Model 12
Pyrite	–	–	–	–	–	–	0.0002	0.0002	0.0002	0.0002	0.0002	0.0002
Calcite	−5.6155	−5.6978	−5.6155	−5.6978	−7.1010	−9.4156	−5.6185	−5.6974	−5.6185	−5.6974	−7.1041	−9.4147
Dolomite	−0.0823	–	−0.0823	–	1.4032	3.7178	−0.0788	–	−0.0788	–	1.4067	3.7173
Gypsum	8.6468	8.6468	8.6468	8.6468	8.6468	8.6468	8.6464	8.6464	8.6464	8.6464	8.6464	8.6464
Albite	3.2039	3.2039	3.2039	3.2039	3.2039	3.2039	3.2039	3.2039	3.2039	3.2039	3.2039	3.2039
K-feldspar	0.0155	0.2131	0.0155	0.2131	3.5807	9.1358	0.0178	0.2070	0.0178	0.2070	3.5831	9.1286
Halite	2.1025	2.1025	2.1025	2.1025	2.1025	2.1025	2.1025	2.1025	2.1025	2.1025	2.1025	2.1025
Biotite	0.0025	0.0025	0.0025	0.0025	0.0025	0.0025	0.0002	0.0002	0.0002	0.0002	0.0002	0.0002
Kaolinite	−5.0508	−4.7709	–	–	–	–	−5.0508	−4.7828	–	–	–	−15.1847
Illite	–	−0.3293	–	−0.3293	−5.9421	−15.2005	–	−0.3154	–	−0.3154	−5.9421	–
Iron Hydroxide	−0.0033	−0.0033	−0.0033	−0.0033	−0.0033	−0.0033	–	–	–	–	–	–
SiO_2	–	–	−10.1016	−9.5418	–	15.7393	–	–	−10.1016	−9.5655	–	15.7124
CO_2	3.8001	3.7178	3.8001	3.7178	2.3146	–	3.7962	3.7173	3.7962	3.7173	2.3106	–

– no mass transfer

[a] All mass transfers are in mmol/l. Models 1 and 2 are the most plausible model of geochemical evolution. Models 3–6 are less possible because the stable product of weathering granitoid is not kaolinite. Models 7–12 can be ignored because pyrite reduction is not significant

geochemical analysis. Based on the concept of water–rock interaction, geochemical interpretation is an effective way to evaluate groundwater resources in a fractured rock aquifer. The stable isotopes of hydrogen and oxygen cluster along Taiwan's LMWL, which reveals an evaporation process under high humidity. However, the amount of precipitation in Kinmen Island is 30% less than evaporation; therefore, infiltration must be fast enough to prevent considerable evaporation. This means the fractured granitoid could be a potential water source for Kinmen Island. The geochemical properties of groundwaters in the granitoid aquifer are principally characterized by SO_4 content. Seawater mixing is first excluded because SO_4 and Cl do not have a linear relationship. NetpathXL is employed to simulate the predominant geochemical reactions controlling chemical evolution of the groundwater. The results demonstrate that the major source of SO_4 is gypsum dissolution rather than pyrite oxidation and the alteration of albite to kaolinite is the dominant reaction characterizing the geochemical properties of deep groundwater.

Acknowledgments This study is supported by research grants from Taiwan Power Company.

References

Beaucaire C, Gassama N, Tresonne N, Louvat D (1999) Saline groundwaters in the hercynian granites (Chardon Mine, France): geochemical evidence for the salinity origin. Appl Geochem 14:67–84

Chen JC (1984) Geochemistry of granite gneiss from Chinmen. Acta Oceanogr Taiwan 15:39–52

Chen PY, Wang MK, Yang DS, Chang SS (2004) Kaolin minerals from Chinmen Island (Quemoy). Clays Clay Miner 52(1):130–137

Clark I, Fritz P (1997) Environmental isotopes in hydrology. CRC Press, Boca Raton

Coleman ML, Shepherd TJ, Durham JJ, Rouse JE, Moore GR (1982) Reduction of water with zinc for hydrogen isotope analysis. Anal Chem 54:993–995

Rechang Consulting Company (2002) Setup groundwater observation well in Kinmen. Kinmen County Government (in Chinese)

Craig H, Gordon L, Horibe Y (1963) Isotopic exchange effects in the evaporation of water: low-temperature experimental results. J Geophys Res 68:5079–5087

Epstein S, Mayeda T (1953) Variation of O-18 content of waters from natural sources. Geochim Cosmochim Acta 4:213–224

Gascoyne M (1994) Hydrogeochemistry, groundwater ages and sources of salts in a granitic batholith on the Canadian Shield, southeastern Manitoba. Appl Geochem 19:519–560

Jalali M (2005) Major ion chemistry of groundwaters in the Bahar area, Hamadan, western Iran. Environ Geol 47:763–772

Jalali M (2007) Assessment of the chemical components of Famenin groundwater, western Iran. Environ Geochem Health 29:357–374

Lan CY, Chung SL, Mertzman SA (1997) Mineralogy and geochemistry of granitic rocks from Chinmen, Liehyu and Dadan Islands, Fujian. J Geol Soc China 40:527–558

Lin W, Chen C-H, Lee CY (1997) Origin of REE-depleted leucogranites in Chinmen Island, SE Fujian. J Geol Soc China 40:587–606

Liu KK (1984) Hydrogen and oxygen isotopic compositions of meteroic waters from the Tatun Shan area, northern Taiwan. Bull Inst Earth Sci Acad Sin 4:159–175

Liu CW, Lin CN, Jang CS, Chen CP, Chang JF, Fan CC, Lou KH (2006) Sustainable groundwater management in Kinmen. Hydrol Processes 20:4363–4372

Liu CW, Jang SC, Chen CP, Lin CN, Lou KL (2008) Characterization of groundwater quality in Kinmen Island using multivariate analysis and geochemical modelling. Hydrol Processes 22:376–383

Parkhurst DL, Appelo CAJ (1999) User's Guide to PHREEQC (Version 2)—a computer program for speciation, batch-reaction, one dimensional transport, and inverse geochemical calculations, water-resources investigations Report 99–4259. US Geological Survey, Reston

Parkhurst DL, Charlton SR (2008) NetpathXL-An Excel interface to the program NETPATH, Techniques and Methods 6-A26. US Geological Survey, Reston

Peters T (1986) Structurally incorporated and water extractable chlorine in the Boettstein granite (N. Switzerland). Contrib Mineral Petrol 94:272–273

Plummer LN, Prestemon EC, Parkhurst DL (1994) An interactive code (NETPATH) for modeling net geochemical reactions along a flow path, version 2.0, Water Resources Investigations Report 94-4169. US Geological Survey, Reston

Stober I, Bucher K (1999) Deep groundwater in the crystalline basement of the Black Forest region. Appl Geochem 14:237–254

Tardy Y (1971) Characterization of the principal weathering types by the geochemistry of waters from some European and African crystalline massifs. Chem Geol 7:253–271